Journal of Applied Physics

RESEARCH ARTICLE | JUNE 17 2024

Determination of band offsets at the interfaces of NiO, SiO_2, Al_2O_3, and ITO with AlN

Hsiao-Hsuan Wan ; Jian-Sian Li ; Chiao-Ching Chiang ; Xinyi Xia ; David C. Hays; Nahid Sultan Al-Mamun ; Aman Haque ; Fan Ren ; Stephen J. Pearton

J. Appl. Phys. 135, 235301 (2024)
https://doi.org/10.1063/5.0214291

04 September 2024 19:06:56

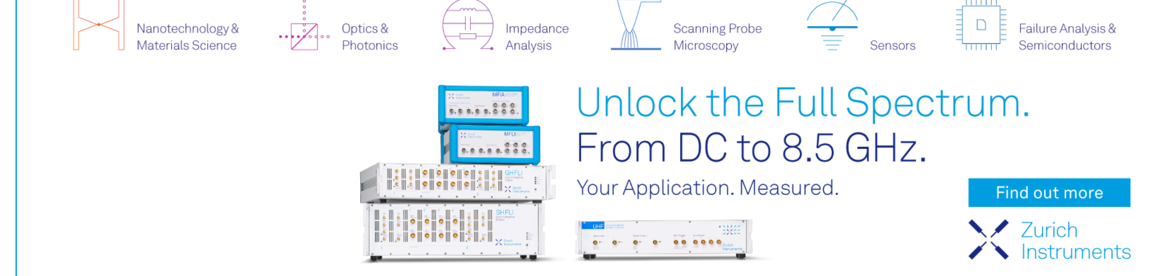

Journal of Applied Physics ARTICLE pubs.aip.org/aip/jap

Determination of band offsets at the interfaces of NiO, SiO_2, Al_2O_3, and ITO with AlN

Cite as: J. Appl. Phys. **135**, 235301 (2024); doi: 10.1063/5.0214291
Submitted: 16 April 2024 · Accepted: 3 June 2024 ·
Published Online: 17 June 2024

Hsiao-Hsuan Wan,[1,a)] Jian-Sian Li,[1] Chiao-Ching Chiang,[1] Xinyi Xia,[1] David C. Hays,[2] Nahid Sultan Al-Mamun,[3] Aman Haque,[3] Fan Ren,[1] and Stephen J. Pearton[4]

AFFILIATIONS

[1]Department of Chemical Engineering, University of Florida, Gainesville, Florida 32611, USA
[2]Nanoscale Research Facility, University of Florida, Gainesville, Florida 32611, USA
[3]Department of Mechanical Engineering, The Pennsylvania State University, University Park, Pennsylvania 16802, USA
[4]Department of Materials Science and Engineering, University of Florida, Gainesville, Florida 32611, USA

[a)]**Author to whom correspondence should be addressed:** hwan@ufl.edu

ABSTRACT

The valence and conduction band offsets at the interfaces between NiO/AlN, SiO_2/AlN, Al_2O_3/AlN, and ITO/AlN heterointerfaces were determined via x-ray photoelectron spectroscopy using the standard Kraut technique. These represent systems that potentially would be used for p-n junctions, gate dielectrics, and improved Ohmic contacts to AlN, respectively. The band alignments at NiO/AlN interfaces are nested, type-I heterojunctions with a conduction band offset of −0.38 eV and a valence band offset of −1.89 eV. The SiO_2/AlN interfaces are also nested gap, type-I alignment with a conduction band offset of 1.50 eV and a valence band offset of 0.63 eV. The Al_2O_3/AlN interfaces are type-II (staggered) heterojunctions with a conduction band offset of −0.47 eV and a valence band offset of 0.6 eV. Finally, the ITO/AlN interfaces are type-II (staggered) heterojunctions with conduction band offsets of −2.73 eV and valence band offsets of 0.06 eV. The use of a thin layer of ITO between a metal and the AlN is a potential approach for reducing contact resistance on power electronic devices, while SiO_2 is an attractive candidate for surface passivation or gate dielectric formation on AlN. Given the band alignment of the Al_2O_3, it would only be useful as a passivation layer. Similarly, the use of NiO as a p-type layer to AlN does not have a favorable band alignment for efficient injection of holes into the AlN.

© *2024 Author(s). All article content, except where otherwise noted, is licensed under a Creative Commons Attribution (CC BY) license (https://creativecommons.org/licenses/by/4.0/).* https://doi.org/10.1063/5.0214291

04 September 2024 19:06:56

I. INTRODUCTION

AlN has a wide bandgap of ~6.2 eV, can be grown in high-quality bulk crystals up to 4 in. in diameter, and exhibits a high breakdown field of approximately 15 MV cm^{-1}.[1–11] These characteristics, including its high thermal conductivity, make it a compelling option for power electronics necessitating operation under conditions of elevated voltage, temperature, and frequency.[1,5] These applications include dc microgrids and pulsed power weapons, as well as switching and transmission within high-voltage direct current (HV-DC) power grids. Recent advancements in doping AlN, both n-type and p-type, through the creation of impurity bands, suggest its prospects for the commercialization of power electronics.[1,8] Historically, AlN was predominantly regarded as an insulator;[12] however, these recent breakthroughs in achieving elevated n- and p-type doping levels have reignited interest in this material for vertical device applications.

To fully exploit the advantages of AlN, establishment of low-resistance Ohmic contacts,[13] selection of appropriate dielectrics with suitable band offsets to AlN, and implementation of low-damage pattern transfer processes are imperative;[14–16] new approaches to doping are needed.[17,18] To date, there has been surprisingly little study of the band alignment of different materials on AlN, perhaps because it has traditionally been considered an insulator, with little applications to devices except in the form of high Al-content AlGaN alloys.[2,6,7] There have been numerous studies of AlN as a dielectric on substrates like SiC,[19,20] Si,[21–23] and InGaAs,[24] but only a few on band alignments of dielectrics on AlN. Ye *et al.*[24] found a type-II energy band alignment with the conduction band discontinuity ΔE_C of 0.83 eV and ΔE_V of −0.23 eV

between ZrO_2 and AlN. Yang *et al.*[25] reported for the MgO/AlN heterostructures a type-I heterojunction with $\Delta E_V = 0.22$ eV and ΔE_C of 1.45 eV. HfO_2/AlN exhibited a type-II alignment with $\Delta E_V = -0.4$ eV and ΔE_C of 0.8 eV.[26] Amorphous Al_2O_3 deposited on bulk AlN crystals grown by atomic layer epitaxy on sapphire exhibited a type-II alignment with $\Delta E_V = -0.75$ eV and $\Delta E_C = 1.45$ eV.[27]

In this paper, we report on the determination of the band alignment at the interfaces of NiO/AlN, SiO_2/AlN, Al_2O_3/AlN, and ITO/AlN heterointerfaces, determined employing x-ray photoelectron spectroscopy with the conventional Kraut technique.[28–30] These configurations are of interest for potential applications in p-n junctions, gate dielectrics, and interfacial layers to improve Ohmic contacts to AlN, respectively.

II. EXPERIMENTAL

The starting AlN-based templates consisted of 3 μm of AlN grown by Metal Organic Chemical Vapor Deposition on 270 nm AlN buffer layers grown by hydride vapor epitaxy on sapphire substrates. Prior findings have indicated the x-ray rocking curve full width at half maximum (FWHM) for peaks located at 14.2° and 17.75° corresponding to the (0 0 0 2) and (20–24) crystallographic planes, with values of 175 and 192 arc sec, respectively.[31] The Raman scattering spectrum showed phonon peaks at 246, 657, and 889 cm^{-1}, corresponding to the E2 (low), E2 (high), and A1 (LO) phonon modes of wurtzite AlN, respectively. The degree of biaxial strain was assessed by comparing the measured E2 (high) peak with that of strain-free AlN. The E2 (high) peak position obtained (657 cm^{-1}) closely matched that of strain-free AlN, suggesting that the AlN was devoid of strain. Additionally, the full width at half maximum (FWHM) of the E2 (high) peaks at 8.16 cm^{-1}, indicative of excellent crystallinity in AlN.[31] The epi layer was undoped and insulating, with surface roughness <0.5 nm and absorption coefficient <100 cm^{-1} Both thick (200 nm) and thin (1.5 nm) layers of the dielectrics were deposited to measure both bandgaps and core levels on the AlN.

NiO deposition was performed via magnetron sputtering under conditions of 3 mTorr and 100 W of 13.56 MHz power, employing two targets to attain a deposition rate of approximately 0.2 Å s^{-1}.[32] The doping concentration in NiO was constant at a level of 5×10^{18} cm^{-3} was maintained for the band alignment investigations. The mobility of the deposited NiO was <1 cm^2 V^{-1} s^{-1}. Throughout the deposition process, the sample temperature was monitored using temperature-sensitive alloys positioned adjacent to the AlN template, ensuring it remained below 100 °C.

The SiO_2 deposition was carried out by sputtering. The target was SiO_2, and the RF power was 350 W. The deposition rate is 0.21 Å/s, with working pressure at 5 mTorr in pure Ar ambient. The bias voltage is about 220 V during the sputtering process. The Al_2O_3 deposition was also carried out by reactive sputtering in O_2, with an Al target and the RF power was 350 W. The deposition rate is 1.4 Å/s, with working pressure at 10 mTorr in O_2 ratio of 3% in Ar.

ITO deposition was conducted via RF magnetron sputtering at ambient room temperature, utilizing a 3-in. diameter pure ITO target. The RF power applied was set at 125 W, and the sputtering occurred at a working pressure of 5 mTorr within a pure Ar environment. Under these conditions, a direct current (dc) bias around 60 V was observed on the electrode.

To avoid surface contamination, the samples underwent x-ray photoelectron spectroscopy (XPS) measurements without prior exposure to air. For the determination of valence band offsets, XPS survey scans were initially conducted to ascertain the surface chemical composition of NiO, SiO_2, ITO, and AlN, enabling subsequent high-resolution analysis for chemical state indentification.[33–35] The XPS analysis employed a Ulvac PHI Versaprobe II system with a monochromatic, scanning aluminum x-ray source emitting at 1486.6 eV with a power setting of 100 μm, 25 W, and 15 kV. The analysis area of the scanning x-ray microprobe is $100\times 100\,\mu m^2$, with a takeoff angle of 45° and an acceptance angle of ±7°. High-resolution scans were performed with an electron pass energy of 23.5 eV, while survey scans used a pass energy of 187.5 eV. The approximate escape depth of the electrons was calculated at 80 Å.

Charge compensation during XPS measurements was carried out using an electron flood gun and low energy ion gun combination, necessitated by the dielectric properties of the films. However, full elimination of surface charge was not always achieved with the flood gun alone, requiring additional corrections. Charge correction was facilitated by referencing the known position of the adventitious carbon (C C) line in the C 1s spectra at 284.8 eV.[36]

Although our experiments did not reveal significant signs of differential charging between any of the deposited layers and AlN, the possibility of such effects in future investigations involving different oxides, varied oxide thicknesses, or distinct conductivity levels within AlN cannot be discounted.

The standard method pioneered by Kraut[28–30] was used to measure the valence band offsets of the four heterostructures. This is based on measuring the shift in core levels of the thick layers of NiO, SiO_2, Al_2O_3, and ITO when they are deposited as thin layers (2–3 nm) on top of the AlN. The deposited layers must be sufficiently thin that the core levels from both materials in the heterostructure can be detected during the XPS measurement. Specifically, one measures the energy difference between the core level of the individual single layers and AlN and their valence band maximum (VBM). The valence band offset ΔE_V is obtained from the relation

$$\Delta E_V = \left(E^1_{core} - E^1_{VBM}\right) - \left(E^{AlN}_{core} - E^{AlN}_{VBM}\right) - \left(E^1_{core} - E^{AlN}_{core}\right). \quad (1)$$

The corresponding conduction band offsets are then obtained from the valence band offsets and measured bandgaps, through the relation

$$\Delta E_C = E_G^{dielectric} - E_G^{AlN} - \Delta E_V. \quad (2)$$

The bandgaps of the respective materials were obtained from absorption measurements (NiO, ITO[33]), reflection electron energy loss spectroscopy[33–37] (SiO_2, Al_2O_3), or XPS (AlN).

A FEI Talos F200X S/TEM system equipped with an energy dispersive x-ray spectroscopy (EDX) detector was used for obtaining bright field TEM images and EDX data from the NiO/AlN structures. These represent the most likely case where the deposition process might lead to damage in the near-surface region of the

04 September 2024 19:06:56

© Author(s) 2024

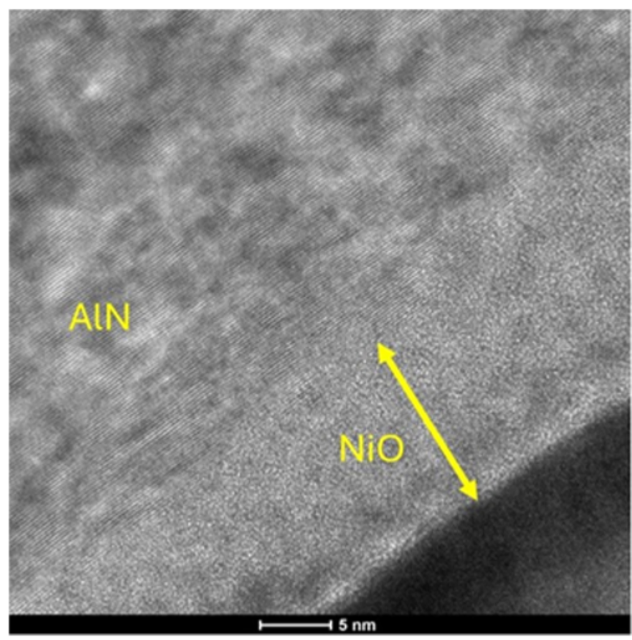

FIG. 1. Cross-sectional TEM images of the NiO deposited on the AlN template.

AlN. The samples were prepared by depositing a protective carbon layer on top of the NiO/AlN structure and a thin Ir layer to prevent charging using an FEI Scios-2 DualBeam FIB system equipped with gallium ion (Ga+) source.

III. RESULT AND DISCUSSION

Figure 1 presents a representative cross-sectional transmission electron microscopy (TEM) image of the NiO layer deposited on the MOCVD grown AlN layer. The interface between the layers was relatively sharp with no discernible extended defects, which suggests the sputtering process effectively mitigated surface damage.

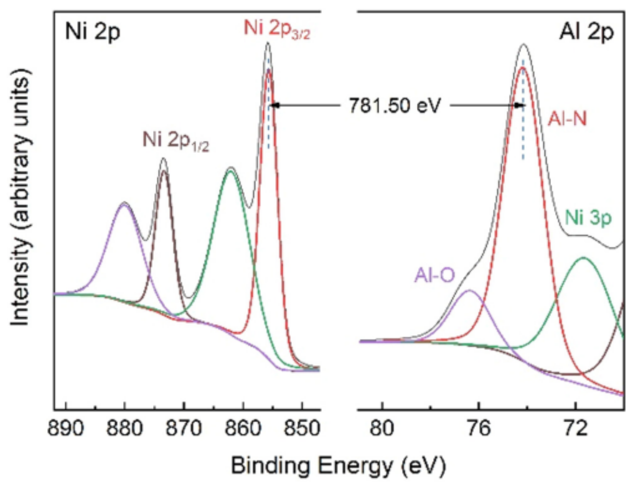

FIG. 3. High resolution XPS spectra for vacuum-core delta energies of thin NiO/AlN heterostructure.

Figure 2 shows the high resolution XPS spectra for the vacuum-core delta regions of AlN using (a) Al 2p and (b) N 1s regions. The bandgap of AlN was determined using the onset of the plasmon loss feature in N 1s photoemission spectrum. The valence band maximum (VBM) was ascertained through linear regression analysis applied to the leading edge of the valence band and the flat energy distribution derived from the XPS measurements. The intersection of these two lines for the AlN template was used for the determination of the VBM.[32] For the AlN, the VBM was 2.79 ± 0.3 eV, core-VBM of 70.61 eV [Fig. 2(a)], and a bandgap of 6.17 eV determined from the N 1s peaks in Fig. 2(c).

NiO has recently been of interest for forming p-n junctions with wider bandgap semiconductors with difficulty in achieving high p-type conductivity, including Ga_2O_3[32] and GaN.[37,38] Figure 3 shows the high resolution XPS spectra for vacuum-core delta energies of thin NiO/AlN heterostructures. Table I gives a summary of

04 September 2024 19:06:56

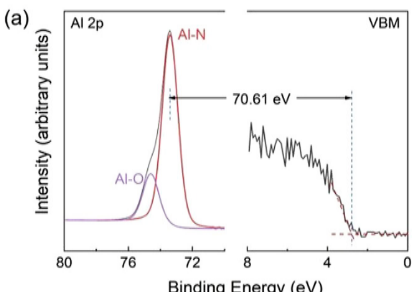

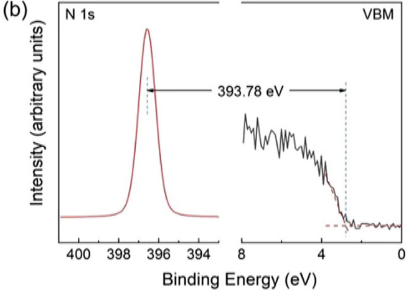

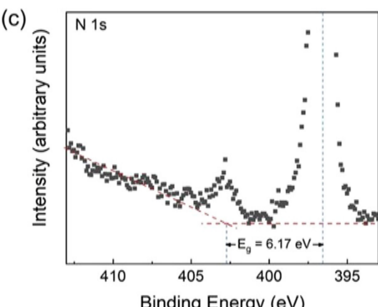

FIG. 2. High resolution XPS spectra for the vacuum-core delta regions of AlN using (a) Al 2p and (b) N 1s regions. (c) Bandgap of AlN determined using the onset of the plasmon loss feature in N 1s photoemission spectrum. The intensities are in arbitrary units (a,u).

© Author(s) 2024

TABLE I. Summary of measured core levels (eV) for bulk AlN, NiO, SiO_2, ITO, and Al_2O_3.

Material	Core level	VBM	Core level peak	Core-VBM	Bandgap
AlN	Al 2p	2.79	73.40	70.61	6.17
	N 1s		396.57	393.78	
NiO	Ni $2p_{3/2}$	−0.6	853.4	854	3.9
SiO_2	Si 2p	4.8	103.5	98.7	8.3
Al_2O_3	O 1s	1.6	529.6	528.0	6.3
ITO	In $3d_{5/2}$	2.74	445.12	442.38	3.5

the measured core levels for AlN and all of the four individual materials investigated for forming heterostructures with the AlN. The corresponding data for the heterostructures are given in Table II, along with the valence and conduction band offsets. Figure 4 shows a schematic of band alignments for NiO/AlN heterostructures. Note that this is a nested, type-I heterojunction with a conduction band offset of −0.38 eV and a valence band offset of −1.89 eV. In other words, this does not seem like a promising approach for making p-n junctions on n-type AlN.

As candidates for dielectrics on AlN-based devices, SiO_2 and Al_2O_3 are the most obvious candidates given that the bandgap has to be larger than that of AlN.[27] Focusing first on SiO_2, Fig. 5 shows high resolution XPS spectra for vacuum-core delta energies of thin SiO_2/AlN heterostructure, while Fig. 6 shows a schematic of band alignments for SiO_2/AlN heterostructure. These spectra were instrumental in identifying core level peak positions. The corresponding values from these spectra are also tabulated in Table I and the derived band offsets are collected in Table II. SiO_2 is a decent candidate as a dielectric for AlN, with a conduction band offset of 1.50 eV, which is significantly higher than the usual rule-of-thumb of desiring at least a 1 eV offset.[39] The valence band offset is smaller, at 0.63 eV, but would still provide a significant barrier to hole conduction.

For Al_2O_3, Fig. 7 shows high resolution XPS spectra for vacuum-core delta energies of thin Al_2O_3/AlN heterostructures, while Fig. 8 shows a schematic of band alignments for Al_2O_3/AlN heterostructure. The smaller bandgap of Al_2O_3 compared to SiO_2 leads to smaller band offsets with AlN, with a value for the conduction band of 0.47 eV and a valence band offset of −0.6 eV. Note that previous reports of band offsets for Al_2O_3 on relatively thin

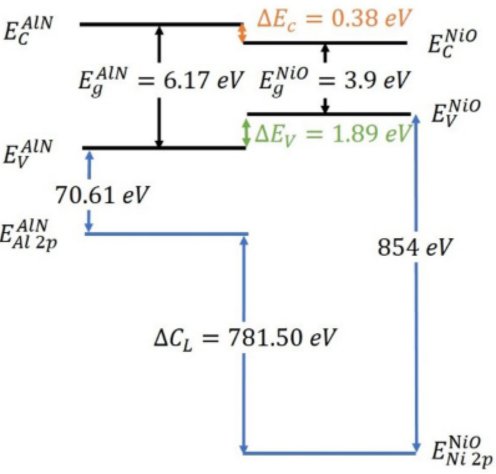

FIG. 4. Schematic of band alignments for NiO/AlN heterostructure.

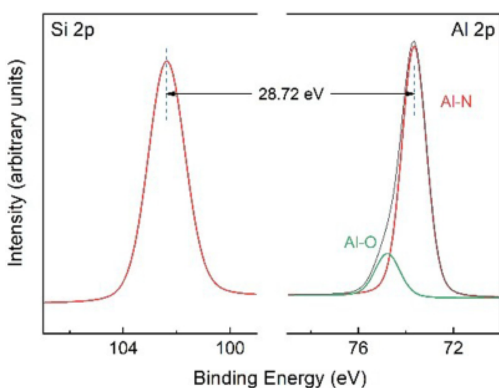

FIG. 5. High resolution XPS spectra for vacuum-core delta energies of thin SiO_2/AlN heterostructure.

04 September 2024 19:06:56

TABLE II. Summary of measured core levels (eV) for AlN heterojunctions with NiO, SiO_2, ITO, and Al_2O_3.

Material	Core level peak (Al 2p)	Core level peak	Δ Core level	ΔE_V	ΔE_C
NiO/AlN	74.16	855.66 (Ni $2p_{3/2}$)	781.50	−1.89	−0.38
SiO_2/AlN	73.65	102.37 (Si 2p)	28.72	0.63	1.50
Al_2O_3/AlN	396.10 (N 1s)	530.92 (O 1s)	134.82	0.6	−0.47
ITO/AlN	72.92	444.75 (In $3d_{5/2}$)	371.83	0.06	−2.73

© Author(s) 2024

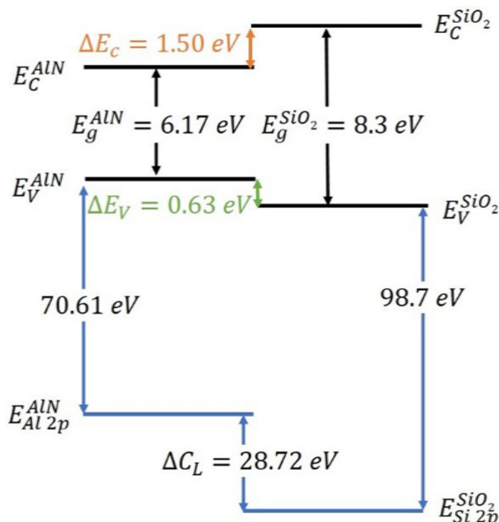

FIG. 6. Schematic of band alignments for SiO_2/AlN heterostructure.

AlN layers grown on sapphire found a type-II alignment with $\Delta E_C = 1.45$ eV and $\Delta E_V = -0.75$ eV.[27] While the overall alignment is the same and the valence band offset is reasonably similar, the conduction band offset is smaller by ~1 eV in our current experiments. Such large differences can arise from the differences in crystalline quality depending on the deposition method, the stoichiometry of the surface, interfacial disorder, thermal history, and surface band bending.[35] These values are less desirable compared to the values for SiO_2 on AlN, indicating that SiO_2 would provide superior carrier confinement in heterostructures. At this point, we have no information on the relative density of interface states in these systems.

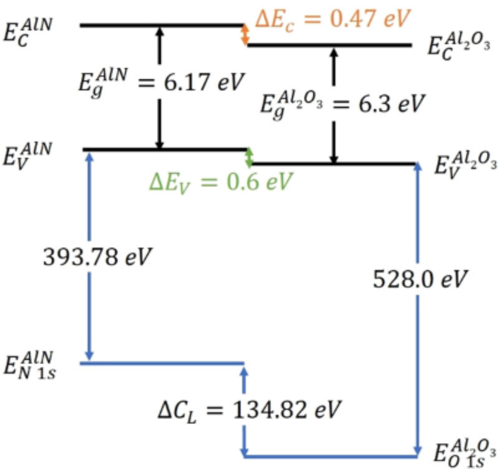

FIG. 8. Schematic of band alignments for Al_2O_3/AlN heterostructure.

For ITO, Fig. 9 shows high resolution XPS spectra for vacuum-core delta energies of thin ITO/AlN heterostructures, while Fig. 10 shows a schematic of band alignments for ITO/AlN heterostructure. The ITO/AlN interfaces are type-II (staggered) heterojunctions with conduction band offsets of −2.73 eV and valence band offsets of 0.06 eV. This indicates that the use of a thin layer of ITO between a metal and the AlN is a potential approach for reducing contact resistance on power electronic devices, where the purpose of the ITO interlayer is to grade the band alignment between the Fermi level of the AlN and a metal contact. Further studies on how annealing affects the alignment are needed, but these findings suggest that in the as-deposited state, ITO exhibits a lower bandgap and favorable band alignment, which could enhance carrier transport across the heterointerface with AlN. Future

04 September 2024 19:06:56

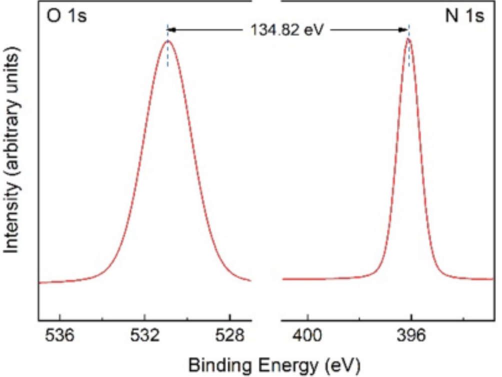

FIG. 7. High resolution XPS spectra for vacuum-core delta energies of thin Al_2O_3/AlN heterostructure.

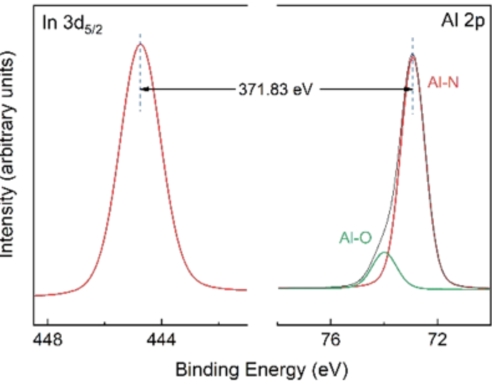

FIG. 9. High resolution XPS spectra for vacuum-core delta energies of thin ITO/AlN heterostructure.

© Author(s) 2024

FIG. 10. Schematic of band alignments for ITO/AlN heterostructure.

investigations should explore the impact of post-deposition annealing on band alignment.

IV. SMMARY AND CONCLUSION

Band alignments at the NiO/AlN, SiO_2/AlN, Al_2O_3/AlN, and ITO/AlN heterojunctions were determined through XPS measurements, revealing nested gap (type I) band offsets for SiO_2 and NiO and staggered, type-II alignments for Al_2O_3 and ITO. Charging and differential charging were not significant issues in our experimental setup and sample configuration. Nevertheless, analytical methodologies for correction,[36,39,40] along with physical methods for electrically isolating the entire sample, offer avenues for mitigating potential concerns. In terms of potential dielectrics materials on AlN, for SiO_2, the valence band offset measured 0.63 eV, while the conduction band offset was determined to be 1.50 eV. The notable conduction band offset contributes to effective electron confinement. Conversely, for Al_2O_3, the valence band offset was found to be −0.6 eV, with a conduction band offset of 0.47 eV. The valence band offset associated with Al_2O_3 does not produce hole confinement. A review of existing literature regarding band offsets for dielectric materials on AlN indicates that SiO_2 emerges as the optimal choice due to its more favorable valence band offset.

The ITO/AlN heterojunction exhibits a nested gap alignment characterized by band offsets, with a valence band offset of −0.06 eV and a conduction band offset of −2.73 eV, as determined through XPS measurements. Introducing ITO interlayers represents an appealing strategy to enhance the contact resistance of Ohmic contacts on n-type AlN layers. Finally, NiO/AlN exhibits a valence band offset of −1.89 eV and a conduction band offset of −0.38 eV, neither of which are favorable from a standpoint of making a p-n unction on n-type AlN. Our results represent a step toward refining some of the processing steps for AlN-based electronic devices.

ACKNOWLEDGMENTS

The work at UF was performed as part of Interaction of Ionizing Radiation with Matter University Research Alliance (IIRM-URA), sponsored by the Department of the Defense, Defense Threat Reduction Agency under Award No. HDTRA1-20-2-0002. The content of the information does not necessarily reflect the position or the policy of the federal government, and no official endorsement should be inferred. A.H. also acknowledges support from the US National Science Foundation (ECCS No. 2015795).

AUTHOR DECLARATIONS

Conflict of Interest

The authors have no conflicts to disclose.

Author Contributions

Hsiao-Hsuan Wan: Data curation (equal); Formal analysis (equal); Investigation (equal); Methodology (equal); Software (equal); Validation (equal); Visualization (equal); Writing – original draft (equal). **Jian-Sian Li:** Investigation (equal); Methodology (equal). **Chiao-Ching Chiang:** Investigation (equal); Methodology (equal). **Xinyi Xia:** Data curation (equal); Investigation (equal); Methodology (equal). **David C. Hays:** Data curation (equal); Methodology (equal); Validation (equal). **Nahid Sultan Al-Mamun:** Formal analysis (equal); Investigation (equal); Methodology (equal); Validation (equal); Visualization (equal). **Aman Haque:** Conceptualization (equal); Funding acquisition (equal); Investigation (equal); Methodology (equal); Validation (equal); Visualization (equal); Writing – review & editing (equal). **Fan Ren:** Conceptualization (equal); Funding acquisition (equal); Project administration (equal); Resources (equal); Supervision (equal); Writing – review & editing (equal). **Stephen J. Pearton:** Conceptualization (equal); Funding acquisition (equal); Project administration (equal); Resources (equal); Supervision (equal); Writing – original draft (equal); Writing – review & editing (equal).

DATA AVAILABILITY

The data that support the findings of this study are available within the article.

REFERENCES

[1]H. Ahmad, Z. Engel, C. M. Matthews, S. Lee, and W. A. Doolittle, J. Appl. Phys. **131**, 175701 (2022).
[2]A. G. Baca, A. M. Armstrong, B. A. Klein, A. A. Allerman, E. A. Douglas, and R. J. Kaplar, J. Vac. Sci. Technol. A **38**, 020803 (2020).
[3]W. A. Doolittle, C. M. Matthews, H. Ahmad, K. Motoki, S. Lee, A. Ghosh, E. N. Marshall, A. L. Tang, P. Manocha, and P. D. Yoder, Appl. Phys. Lett. **123**, 070501 (2023).
[4]A. L. Hickman, R. Chaudhuri, S. J. Bader, K. Nomoto, L. Li, J. C. Hwang, H. Grace Xing, and D. Jena, Semicond. Sci. Technol. **36**, 044001 (2021).
[5]M. Hiroki, Y. Taniyasu, and K. Kumakura, IEEE Electron Device Lett. **43**, 350 (2022).
[6]R. Kaplar, A. A. Allerman, A. Armstrong, M. H. Crawford, J. R. Dickerson, A. J. Fischer, A. Baca, and E. Douglas, ECS J. Solid State Sci. Technol. **6**, Q3061 (2017).

04 September 2024 19:06:56

© Author(s) 2024

[7]A. Kasei, "Crystal IS and Asahi Kasei announce first 4-inch aluminum nitride substrate," Vol. 2023 (2023), available at https://www.asahi-kasei.com/news/2023/e230821.html.
[8]H. Okumura, S. Suihkonen, J. Lemettinen, A. Uedono, Y. Zhang, D. Piedra, and T. Palacios, Jpn. J. Appl. Phys. **57**, 04FR11 (2018).
[9]F. Ren and S. J. Pearton, *Wide Bandgap Semiconductor-Based Electronics* (IOP Publishing, 2020).
[10]J. Tsao, S. Chowdhury, M. Hollis, D. Jena, N. Johnson, K. Jones, R. Kaplar, S. Rajan, C. Van de Walle, E. Bellotti, C. L. Chua, R. Collazo, M. E. Coltrin, J. A. Cooper, K. R. Evans, S. Graham, T. A. Grotjohn, E. R. Heller, M. Higashiwaki, M. S. Islam, P. W. Juodawlkis, M. A. Khan, A. D. Koehler, J. H. Leach, U. K. Mishra, R. J. Nemanich, R. C. N. Pilawa-Podgurski, J. B. Shealy, Z. Sitar, M. J. Tadjer, A. F. Witulski, M. Wraback, and J. A. Simmons, Adv. Electron. Mater. **4**, 1600501 (2018).
[11]M. H. Wong, O. Bierwagen, R. J. Kaplar, and H. Umezawa, J. Mater. Res. **36**, 4601 (2021).
[12]E. Douglas, S. Reza, C. Sanchez, D. Koleske, A. Allerman, B. Klein, A. Armstrong, R. Kaplar, and A. Baca, Phys. Status Solidi A **214**, 1600842 (2017).
[13]B. A. Kazanowska, Thesis, University of Florida, 2021.
[14]A. Azarov, J. G. Fernández, J. Zhao, F. Djurabekova, H. He, R. He, Ø Prytz, L. Vines, U. Bektas, P. Chekhonin, N. Klingner, G. Hlawacek, and A. Kuznetsov, Nat. Commun. **14**, 4855 (2023).
[15]W. Guo, R. Kirste, I. Bryan, Z. Bryan, L. Hussey, P. Reddy, J. Tweedie, R. Collazo, and Z. Sitar, Appl. Phys. Lett. **106**, 082110 (2015).
[16]J. Mileham, S. Pearton, C. Abernathy, J. MacKenzie, R. Shul, and S. Kilcoyne, Appl. Phys. Lett. **67**, 1119 (1995).
[17]M. H. Breckenridge, P. Bagheri, Q. Guo, B. Sarkar, D. Khachariya, S. Pavlidis, J. Tweedie, R. Kirste, S. Mita, and P. Reddy, Appl. Phys. Lett. **118**, 112104 (2021).
[18]Z. Shen, F. Zhang, J. Chen, Z. Fu, X. Liu, G. Yan, B. Lv, Y. Wang, L. Wang, and W. Zhao, Appl. Phys. Lett. **117**, 102105 (2020).
[19]J. Choi, R. Puthenkovilakam, and J. P. Chang, Appl. Phys. Lett. **86**, 192101 (2005).
[20]S. W. King, R. J. Nemanich, and R. F. Davis, J. Appl. Phys. **118**, 045304 (2015).
[21]M. Badylevich, S. Shamuilia, V. Afanas'Ev, A. Stesmans, Y. Fedorenko, and C. Zhao, J. Appl. Phys. **104**, 093713 (2008).
[22]H. B. Do, Q. H. Luc, M. T. H. Ha, C. C. Hu, Y. C. Lin, and E. Y. Chang, IEEE Trans. Electron Devices **62**, 3987 (2015).
[23]K. Stevens, M. Kinniburgh, A. Schwartzman, A. Ohtani, and R. Beresford, Appl. Phys. Lett. **66**, 3179 (1995).
[24]G. Ye, H. Wang, and R. Ji, Appl. Phys. Express **8**, 081002 (2015).
[25]A. Yang, H. Song, X. Liu, H. Wei, Y. Guo, G. Zheng, C. Jiao, S. Yang, Q. Zhu, and Z. Wang, Appl. Phys. Lett. **94**, 052101 (2009).
[26]G. Ye, H. Wang, and R. Ji, Appl. Phys. Lett. **108**, 162103 (2016).
[27]C. Fares, F. Ren, M. J. Tadjer, J. Woodward, M. A. Mastro, B. N. Feigelson, C. R. Eddy, and S. Pearton, Appl. Phys. Lett. **117**, 182103 (2020).
[28]E. Kraut, J. Vac. Sci. Technol. B **5**, 1246 (1987).
[29]E. Kraut, R. Grant, J. Waldrop, and S. Kowalczyk, Phys. Rev. Lett. **44**, 1620 (1980).
[30]E. Kraut, R. Grant, J. Waldrop, and S. Kowalczyk, Phys. Rev. B **28**, 1965 (1983).
[31]Y. Choi, R. Choi, and J. Kim, Appl. Surf. Sci. **509**, 145279 (2020).
[32]J.-S. Li, X. Xia, C.-C. Chiang, D. C. Hays, B. P. Gila, V. Craciun, F. Ren, and S. Pearton, J. Vac. Sci. Technol. A **41**, 013405 (2023).
[33]E. Bersch, M. Di, S. Consiglio, R. Clark, G. Leusink, and A. C. Diebold, J. Appl. Phys. **107**, 043702 (2010).
[34]D. C. Hays, B. Gila, S. Pearton, and F. Ren, Vacuum **122**, 195 (2015).
[35]D. C. Hays, B. Gila, S. Pearton, and F. Ren, Appl. Phys. Rev. **4**, 021301 (2017).
[36]H. C. Shin, D. Tahir, S. Seo, Y. R. Denny, S. K. Oh, H. J. Kang, S. Heo, J. G. Chung, J. C. Lee, and S. Tougaard, Surf. Interface Anal. **44**, 623 (2012).
[37]Y. Ma, M. Xiao, Z. Du, X. Yan, K. Cheng, M. Clavel, M. K. Hudait, I. Kravchenko, H. Wang, and Y. Zhang, Appl. Phys. Lett. **117**, 143506 (2020).
[38]C.-C. Chiang, H.-H. Wan, J.-S. Li, F. Ren, T. J. Yoo, H. Kim, and S. Pearton, J. Vac. Sci. Technol. B **41**, 062205 (2023).
[39]G. Greczynski and L. Hultman, J. Appl. Phys. **132**, 011101 (2022).
[40]G. H. Major, J. W. Pinder, D. E. Austin, D. R. Baer, S. L. Castle, J. Čechal, B. M. Clark, H. Cohen, J. Counsell, and A. Herrera-Gomez, J. Vac. Sci. Technol. A **41**, 038501 (2023).

04 September 2024 19:06:56

© Author(s) 2024